TTC 2013
6th ESA International Workshop on Tracking, Telemetry
and Command Systems for Space Applications ESA-ESOC, 10 - 13 September 2013

INVESTIGATING KA-BAND SCIENCE DATA TRANSFER FOR BEPICOLOMBO MISSION BY USING RADIOMETEOROLOGICAL NUMERICAL MODELS

F.S. Marzano[1,3,5], M. Biscarini[1,3], L. Iess[2,3], M. Montopoli,[4,5] K. De Sanctis[5,6], M. Gregnanin[2,7], M. Parisi[2,7], M. Montagna[8], E. Montagnon[8], M. Arza[8], M. Mercolino[8], M. Lanucara[8]

[1] *DIET, Sapienza University of Rome, Italy*
[2] *DIMA, Sapienza University of Rome, Italy*
[3] *CRAS, Sapienza University of Rome, Italy*
[4] *DG, University of Cambridge, UK*
[5] *CETEMPS, University of L'Aquila, Italy*
[6] *HIMET, L'Aquila, Italy*
[7] *ARPSoft, Rome, Italy*
[8] *ESOC, European Space Agency, Germany*

I. INTRODUCTION

Deep space (DS) exploration is aimed at acquiring information about the solar system and its composition, a purpose that can be achieved only if a significant communication capacity can be provided to spacecrafts at very large distances [1]. The Ka-band (at 32-34 GHz) and higher frequency band channels can provide this capacity if compared to the current X-band (around 8.4 GHz) [2]-[4]. Ka-band can offer a striking performance advantage over X-band because of the *square-frequency* law increase of directivity of the downlink beam for the same physical antenna size. This opens up a possible and useful trade space for Ka-band missions with the same antenna size (and spacecraft constraints) and radio frequency power, since a Ka-band mission can return four times more data than a comparable X–band mission. For the European Space Agency (ESA), the next step in this direction will be the utilisation of Ka-band downlinks both to generate radiometric observables (in combination with X-band uplink) as well as to increase science data transfer [5]. The first satellite mission adopting such frequency operationally will be BepiColombo (BC), the ESA cornerstone mission to Mercury (expected launch in 2015) including the Mercury Orbiter Radio Experiment (MORE) at X-Ka band [6].

The optimal allocation of channel resources above Ku band is limited by the significant impact of radio-meteorological factors which can irremediably degrade the quality of service for fairly high percentage of time [7]. At Ka band, for instance, attenuation due to cloudy and rainy troposphere can be even one order of magnitude larger than at X-band. The major cause of outages at Ka band and above is due to rainfall, as well as non-precipitating clouds. For small carrier-to-noise ratio (CNR), the impact of atmospheric noise temperature can become non-negligible [4]. In order to achieve the optimum data return at Ka-band, a different approach with respect to the link budget computation at lower frequencies (e.g., S or X band) is necessary [2]. Such link analysis is based on the maximization of the expected data return in a probabilistic framework rather than on a specified link statistical availability. Recent methods uses monthly statistics collected at the receiving site with the aim of defining average values of expected received data volume [5] and the exploitation of numerical weather forecasting is also foreseen [3].

This paper introduces the preliminary concept of the RadioMetOP (RadioMeteorological Operations Planner) technique and describes its main modelling components and objectives, limiting the analysis to rainfall effects. Numerical results in terms of received frame data for unconstrained and constrained system scenarios are also described together with a discussion about the possible impact of RadioMetOP methods on BC operations.

II. PHYSICAL-STATISTICAL MODELING OF THE RADIOMETEOROLOGICAL CHANNEL

The *link budget basic formula* can be compactly expressed as follows (e.g., [2], [5]):

$$\frac{E_b}{N_0} = f_{\mathrm{ENR}}\left\{C_{TX}, C_{RX}, \lambda, \theta(t), R_b(t), r(\theta), \mathbf{x}_{atm}(t), L_{atm}(r,\lambda,\mathbf{x}_{atm}), T_{atm}(r,\lambda,\mathbf{x}_{atm})\right\} \quad (1)$$

where f_{ENR} is the Friis function for the energy-per-bit-to-noise-density ratio E_b/N_0 (ENR), C_{TX} is the transmitter constant, C_{RX} is the receiver constant, λ is the carrier wavelength, θ is the antenna elevation angle variable with time t (temporal profile of the antenna elevation angle), R_b is the bit rate, r is the slant range, $\mathbf{x}_{atm}$ the atmospheric spatial state vector, L_{atm} is the atmospheric path loss and T_{atm} the atmospheric equivalent noise temperature. The *atmospheric state vector* $\mathbf{x}_{\mathrm{atm}}$ is defined for any point *(x,y,z)* and time *t*. It includes both thermodynamic variables (such as pressure, temperature, humidity and wind velocity and orientation) and microphysical variables (such as the atmospheric particle concentration of water clouds and aerosol dispersions). Its knowledge can be acquired through:

- *Experimental measurements* using in situ instruments (e.g., the raingauge able to measure the accumulated rainfall intensity at ground and the radiosonde able to measure thermodynamic profiles) and/or remote sensing instruments (e.g., microwave radiometers for estimating integrated water contents and temperature profiles and weather radars for estimating rainfall intensity and hydrometeor distribution) [8];
- *Numerical models* which can predict the meteorological state variables by using proper initial and boundary conditions by solving the so called "primitive" weather differential equations in a given domain (from several tens to thousands of kilometres, depending on the model scale) and for a lead time up to several days, eventually assimilating measured data [9].

In a given period of time and in a given spatial domain the atmosphere can be considered a *random process* from the perspective of radiometeorology. Its state $\mathbf{x}_{atm}$ can be thought as a realization of a vector random variable $\mathbf{X}_{atm}$, characterized by a multidimensional *probability density function (PDF)* $p_X(\mathbf{x}_{atm})$ and its associated statistical moments (e.g., multidimensional average vector and covariance matrix). If the atmospheric state is reduced to the rainfall intensity or rate R (mm/h), then we have $p_R(R)$. For radiopropagation purposes it is also worth introducing the distribution function associated to a PDF. If X is a scalar random variable with PDF $p_X(x)$ being x a random realization of the process, we can define the *cumulative distribution function* (CDF) $D(x)$ and its complementary function, also called the *cumulative survival function* (CSF) $S(x)$, as follows:

$$D_X(x) = \int_{-\infty}^{x} p_X(x')dx' = \Pr(X \le x); \quad S_X(x) = \int_{x}^{\infty} p_X(x')dx' = \Pr(X \ge x) = 1 - D(x) \tag{2}$$

where Pr is the probability function. The randomness of the atmosphere implies that all the variables depending on $\mathbf{x}_{atm}$, such as L_{atm} and T_{atm}, becomes random functions with PDF expressed by $p_L(L_{atm})$ and $p_T(T_{atm})$.

The functional relations of L_{atm} and T_{atm} on the geometry and atmospheric optical parameters can be explicitly expressed as [7], [8], [4]:

$$\begin{cases} L_{atm}(r,\lambda,\mathbf{x}_{atm}) = e^{-A(r,\lambda,\mathbf{x}_{atm})} = e^{-\int_0^{r_0}\alpha(r,\lambda,\mathbf{x}_{atm})dr} \\ T_{atm}(r,\lambda,\mathbf{x}_{atm}) = T_m(\lambda,\mathbf{x}_{atm};\mathbf{w}_{atm},\mathbf{g}_{atm})\left[1 - L_{atm}(r,\lambda,\mathbf{x}_{atm})\right] \end{cases} \tag{3}$$

where A is the slant path attenuation and α is the specific attenuation, T_m is the mean radiative temperature with $\mathbf{w}_{atm}$ and $\mathbf{g}_{atm}$ the atmospheric volumetric albedo and asymmetry factor vectors. The evaluation of L_{atm} and T_{atm} can be carried out by means of:

- *Simplified radiative models (SRM)* approximating $\mathbf{x}_{atm}$ through R (the dominant atmospheric component which is here considered) and then using a layering up to the freezing height H_0 (eventually estimated from surface temperature T_s and vertical thermal gradient ∇T) coupled with an effective length factor due to horizontal finite extension of convective precipitation and a specific attenuation model depending on R (i.e., $\alpha = aR^b$):

$$A(r,\lambda,\mathrm{R}) = \alpha(\lambda,\mathrm{R})\Delta r = a(\lambda)R^{b(\lambda)}\left[H_0(T_s,\nabla T) - H_s\right]\mathrm{cosec}(\theta); \quad T_m(\lambda,\mathrm{R};w_{atm},g_{atm}) = T_{m0} \tag{4}$$

where H_s is the surface height, "cosec" the cosecant function and T_{m0} is an average temperature [7].

- *Radiative transfer models (RTM)* where from the atmospheric state $\mathbf{x}_{atm}$ both the path attenuation and the atmospheric noise temperature can be derived by taking into account the gaseous absorption, the microphysical properties of cloud droplets and hydrometeors by estimating $\mathbf{w}_{atm}$ and $\mathbf{g}_{atm}$ [4];
- *Microwave radiometric measurements* at ground, carried out at the frequency of the microwave link possibly collocated with the receiving antenna [8].

In this paper we will concentrate on the SRM approach, as a first-guess modelling framework.

A. *Microwave link performance parameters*

During the Earth-satellite data transmission, the *frame error rate (FER)* should be taken into account and related to the ratio E_b/N_0 depending on the adopted coding scheme f_{FER}:

$$FER(t) = f_{FER}\left\{\frac{E_b}{N_0}[\theta(t),\mathrm{R}_b(t),\mathbf{x}_{atm}(t)]\right\} \tag{5}$$

where the dependence of E_b/N_0 has been reduced for simplicity to the basic degree of freedom. Once FER is known and a continuous satellite pass of duration Δt is set, the *number of the transmitted frames F_{TX}, lost frames F_{LX} and received frames F_{RX}* is given by:

$$\begin{cases} F_{TX} = \dfrac{\mathrm{R}_b}{r_B}\Delta t; \quad F_{LX} = \displaystyle\int_{\Delta t} F_{LX}(t)dt = \frac{\mathrm{R}_b}{r_B}\int_{\Delta t} f_{FER}\left\{\theta(t),\mathrm{R}_b(t),\mathbf{x}_{atm}(t)\right\}dt; \quad F_{LX\%} = 100\dfrac{F_{LX}}{F_{TX}} \\ F_{RX} = F_{TX} - F_{LX} = \dfrac{\mathrm{R}_b}{r_B}\Delta t - \dfrac{\mathrm{R}_b}{r_B}\displaystyle\int_{\Delta t} f_{FER}\left\{\theta(t),\mathrm{R}_b(t),\mathbf{x}_{atm}(t)\right\}dt \end{cases} \tag{6}$$

where r_B is the frame block length. The *percentage fractional number of the lost frames* $F_{LX\%}$ can be an important parameter for close-loop file transfer protocols [5].

The fact that $\mathbf{x}_{atm}$ is a random variable in given time-space domain implies that that F_{LX} and F_{RX} are random function as well, characterized by PDF expressed by $p_{LX}(F_{LX})$ and $p_{RX}(F_{RX})$. This consideration opens the possibility to derive the statistical moments of these stochastic processes such as the *mean value*:

$$\begin{cases} < F_{LX} >= \int_{-\infty}^{\infty} f_{LX}\, p_{LX}(f_{LX}) df_{LX} = \dfrac{R_b}{r_B} < \int_{\Delta t} f_{FER}\{\theta(t), R_b(t), \mathbf{x}_{atm}(t)\} dt > \\ < F_{RX} >= F_{TX} - < F_{LX} >= \dfrac{R_b}{r_B}\Delta t - \int_{-\infty}^{\infty} f_{LX}\, p_{LX}(f_{LX}) df_{LX} \end{cases} \quad (7)$$

where "<>" indicates the ensemble average operator.

B. *Input data and system constraints for BepiColombo mission*

Any deep-space mission, such as BC, is designed within data-transmission system specification and operational constraints in order to match at best with science requirements [6]. The most important ground system data are typically the following: i) antenna site latitude (lat_A) and longitude (lon_A) [°]; ii) carrier wavelength λ [m]; iii) satellite pass interval Δt [h] with its possible interruptions, its j-th sub-pass Δt_{subj} [s] out of N and a discretization δt; iv) temporal profile of the antenna elevation angle θ(t) [°] within a pass interval Δt and a time discretization; v) temporal profile of the link range r(t) [km] within a pass interval Δt. The most important Earth-satellite link system constraints are: i) bit rate R_b (b/s) is discretized into i-th values R_{bi} belonging to a predefined set ΔR_b of size M; ii) bit-rate R_b (b/s) is constant within each pass or sub-pass; iii) elevation angle θ(t) can be varied between a minimum θ_m and a maximum θ_M (depending on the pass interval) iv) FER function defined by the Turbo code scheme (¼ and/or ½); v) operations are planned 12 till 72 hours in advance.

The following Table 1 summarizes the main BC system specifications [5].

Table 1: Spacecraft and ground station main parameters for the BC link budget

PARAMETER	VALUE	PARAMETER	VALUE
Link central frequency	32.01 GHz	Modulation losses $L_{mod\|dB}$	0.54 dB
Satellite $EIRP_{SC\|dB}$	58.26 dBW	Pointing losses $L_{pr\|dB}$	0 dB
Cebreros latitude	40.45°	Antenna gain $G_{r\|dB}$ (incl. pointing loss)	76.94 dB
Cebreros longitude	-4.37°	System noise temperature T_{sys} (at 10°, 25% CD)	21.14 dBK
Cebreros height (ASL)	0.760 km	Physical temperature T_0	300 K
Receiving antenna diam.	35 m	Collected ground noise T_{gr}	22.2 K
Demodulation losses $L_{dem\|dB}$	For Turbo ¼: 0.89-1.00 dB For Turbo ½: 0.72 dB	Noise temperature T_r	32.4 K
		Feed losses L_{fr}	0.29 dB

Input meteorological data for given given site can be derived from: i) ITU-R climatological statistics available from the radio database; ii) Experimental rain gauge precipitation rate R (mm/h) together with surface pressure p_s (hPa), temperature T_s (K) and specific humidity q_s (kg/kg); iii) Modelled rain rate expressed as R (mm/h) together with surface pressure p_s (hPa), temperature T_s (K) and specific humidity q_s (kg/kg); iv) Modelled atmospheric state as a 3D variable vector. In this paper we will focus on the ITU-R input data and on the Cebreros rain gauge meteorological time series, including both rainfall intensity and surface temperature.

III. DATA RETURN ESTIMATION METHODOLOGIES

Maximization of science data return in deep space missions is a major task [2]. In order to properly designing the satellite and Earth receiving-transmitting modulation, there is the need to estimate retrievable data volume as accurate as possible taking into account the randomly varying Earth atmosphere [3]-[5]. This basically translates into the goal of predicting the data bit rate R_b and antenna elevation excursion θ.

Two estimation methods to derive the link parameters are here considered and named: i) conventional approach; ii) statistical approach. For both approaches we will assume to know the CDF of both the atmospheric path attenuation loss L_{atm} and the antenna noise temperature T_{atm} on a given timeframe (month or year). To be general we will deal with both optimization variable R_b and θ_m for the whole pass Δt (for each subpass the extension is obvious: $\Delta t=\Delta t_i$). From (2), atmospheric CDFs of interest are expressed by:

$$D_L(l_{atm}) = \int_{-\infty}^{l_{atm}} p_L(l')dl' = \Pr(L_{atm} \le l_{atm}); \quad D_T(t_{atm}) = \int_{-\infty}^{t_{atm}} p_T(t')dt' = \Pr(T_{atm} \le t_{atm}) \quad (8)$$

A. *Conventional approach*

The rationale of this approach is based on the on the conventional telecommunication link design techniques, taking into account the ENR margin. The foreseen steps are:

- If necessary (e.g., when having only surface rain rates), assume a simplified radiative model (SRM), as in (4), for the angular dependence of L_{atm} on $\theta(t)$ with respect to the zenithal path attenuation A_z.
- Select the CDFs D_L and D_T of L_{atm} and T_{atm}, respectively, for a desired timeframe and data source.
- Set the CDF at the desired probability p_{atm} or percentage probability (e.g., 90%) so that l_{atmp} and t_{atmp}:

$$D_L(l_{atmp}) = 100 p_{atm}; \qquad D_T(t_{atmp}) = 100 p_{atm} \tag{9}$$

  In case D_T is not available (or viceversa D_L is not available), then use SRM from (4) with $L_{atm}=l_{atmp}$ (or $T_{atm}=t_{atmp}$). Values of l_{atmp} and t_{atmp} can be function of θ using (4).
- Set the margin or threshold ENR_{th} (e.g., 3 dB) to be added to the coding threshold derived from (5);
- Using the link budget formula in (1), invert it in order to find the *"conventional" solution couple R_{bic} and θ_{mc}*, that is the discrete bit rate R_{bic} within ΔR_b and minimum scanning elevation θ_{mc} within $\Delta\theta$, by varying the temporal profile of $\theta(t)$ within the pass Δt with the constraint $ENR \geq ENR_{th}$ *(e.g., ½ or 3 dB)*:

$$ENR_{th} \leq f_{ENR}\{\theta_{mc}, R_{bic}; \theta(t), l_{atmp}(\theta), t_{atmp}(\theta)\} \tag{10}$$

- Using the *"conventional" solution couple R_{bic} and θ_{mc}* compute:

$$F_{LX\%} = \frac{100\, R_{bic}}{F_{TX}\, r_B} \int_{\Delta t} f_{FER}\left\{ f_{ENR}\{\theta_{mc}, R_{bic}; \theta(t), l_{atmp}(\theta), t_{atmp}(\theta)\}\right\} dt \tag{11}$$

- Estimate the lost frames F_{LX} and received frames F_{RX} by means of:

$$F_{LX} = F_{TX}\frac{F_{LX\%}}{100} = \left(\frac{R_{bic}}{r_B}\Delta t\right)\frac{F_{LX\%}}{100}; \quad F_{RX} = F_{TX} - F_{LX} = \frac{R_{bic}}{r_B}\Delta t - F_{LX} \tag{12}$$

  Note that Δt should be reduced by taking into account the effective transmission sub-pass intervals and the condition $\theta(t) \geq \theta_{mc}$.

B. *Statistical approach*

The rationale of this approach is based on the combination between the conventional approach and the statistical evaluation of the number of the received frames. The foreseen steps are similar to those of the conventional approach, but after finding the *"statistical" solution couple $R_{bis}=R_{bic}$ and $\theta_{ms}=\theta_{mc}$*, the estimate of the received frames is carried out in a statistical sense:

- Estimate the PDFs of L_{atm} and T_{atm} from their CDFs through proper normalization constants c_L and c_T:

$$\begin{cases} S_L(l_{atm}) = 1 - D_L(l_{atm}); & p_L(l_{atm}) = c_L \Delta D_L(l_{atm}) / \Delta l_{atm} \\ S_T(t_{atm}) = 1 - D_T(t_{atm}); & p_T(t_{atm}) = c_T \Delta D_T(t_{atm}) / \Delta t_{atm} \end{cases} \tag{13}$$

- Estimate the average <FER> within the pass Δt from the following expression:

$$< FER(t) >=< f_{FER}\{ENR(t, L_{atm})\} >= \int_0^\infty f_{FER}\, p_{FER}(f_{FER})\, df_{FER} = \int_0^\infty f_{FER}(l_{atm})\, p_L(l_{atm})\, dl_{atm} \tag{14}$$

  where p_{FER} is the PDF of FER and it holds the following equality [5]:

$$p_{FER}[f_{FER}(l_{atm})]\, df_{FER}(l_{atm}) = p_L(l_{atm})\, dl_{atm} \tag{15}$$

- Estimate the average lost frames <F_{LX}>, percentage lost frames <$F_{LX\%}$> and received frames <F_{RX}>:

$$\begin{cases} < F_{LX} >= \dfrac{R_{bi}}{r_B} < \int_{\Delta t} FER(t)\, dt >= \dfrac{R_{bi}}{r_B} \sum_{n=1}^{N_{int}} \int_{\tau_n} < FER(\Delta_{tn}) > dt = \dfrac{R_{bi}}{r_B} \sum_{n=1}^{N_{int}} \left[< FER(\Delta_{tn}) > \Delta_{tn} \right] \quad \text{with} \sum_{n=1}^{N_{int}} \Delta_{tn} = \Delta t \\ < F_{RX} >= F_{TX} - < F_{LX} > \cong \dfrac{R_{bi}}{r_B}\Delta t - \dfrac{R_{bi}}{r_B} \int_{\Delta t} < FER(t) > dt \end{cases} \tag{16}$$

IV. DATA ANALYSIS FOR CEBREROS GROUND STATION

As already mentioned, in this work we will mainly focus on the Ka-band rainfall effects along BC Earth-satellite link. The Cebreros station (lat. 40° 27' 09.68", lon. -04° 22' 03.18",) is an ESTRACK (European Space Tracking network, operated by ESOC-ESA) radio antenna, located 90 km from Madrid (Spain). A 35-metres diameter antenna (DSA-2: Deep Space Antenna 2), operating at X- and Ka-bands, is hosted.

Fig. 1 shows the meteorological measurements acquired in Cebreros (Spain) in 2012 together with their CDF. Note the seasonal variation of surface temperature which impacts on the standard freezing level height in (4), using a gradient ∇T of 6.5 °/km. In 2012 the most rainy months were September (cumulative rain of 77 mm) and November (72 mm) and the least was August (< 1 mm).

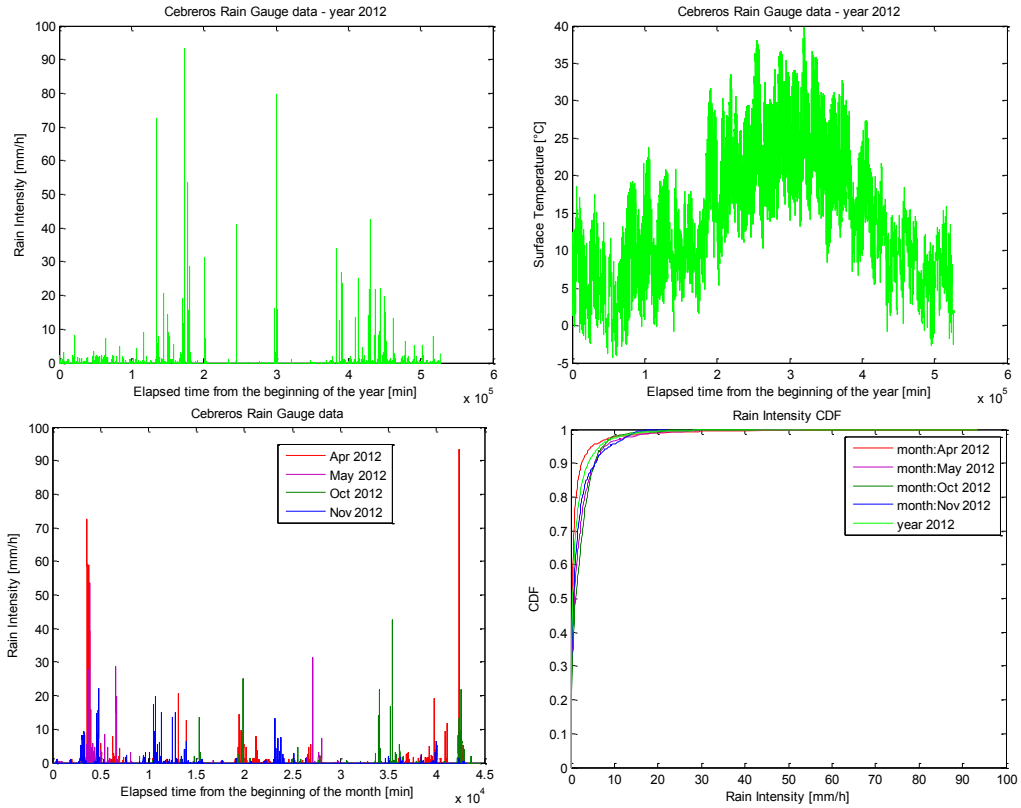

Fig. 1. Rain gauge and temperature time series for year 2012 and months April-May-October-November 2012 together with (bottom right) CDF of rain intensity (R>0) for year 2012 and months April- May-October-November

By using the SRM in (4) and SNEM power-law attenuation-rainfall coefficients [8], Cebreros rain measurements of Fig. 1 have been converted into rain path attenuations at zenith (elevation angle of 90°), as shown by Fig. 2, in terms of corresponding time series and CDFs. The instantaneous elevation dependence is assumed to follow a cosecant law as in (4) [7].

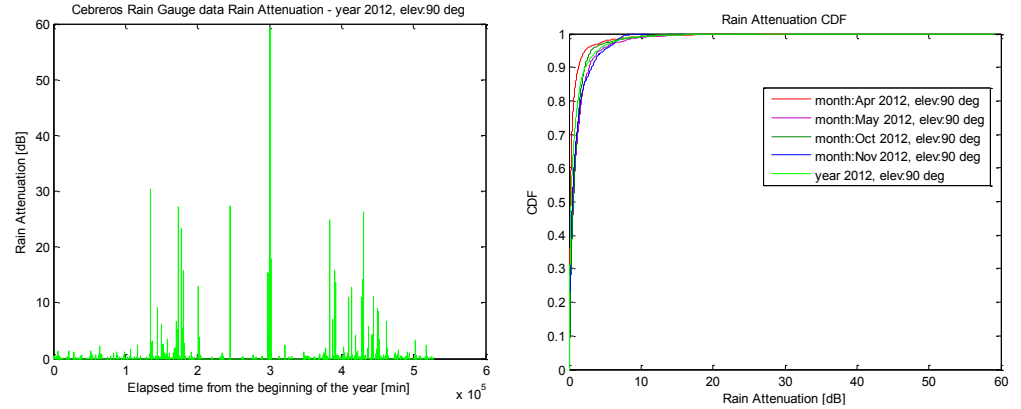

Fig. 2. Time series of Ka-band modelled rain path attenuation for year 2012 and CDF of rain path attenuation for year 2012 and months April-May-October-November at 90° elevation.

In order to have a reference, the ITU-R rain path attenuation probabilistic model at Ka band has been applied on a yearly basis (using both climatological and gauge R_{001} value relative to 0.01% of rainfall CSF). CDFs are shown in Fig. 3 for the various atmospheric components (rain, cloud, water vapour, total) at 90° elevation [10]. Note that, due to the Cebreros large antenna diameter, the scintillation aperture averaging factor is almost zero thus proving a negligible scintillation log-amplitude variance contribution [7].

V. NUMERICAL EVALUATION OF BEPICOLOMBO DATA RETURN

In order to evaluate the accuracy of the data return estimation capability, we need to set up a benchmark test case. The latter is defined as the ideal transmitting approach with no system constraints (fully adaptive R_b changeable at each elevation angle step fulfilling the ENR margin) and in presence of a perfect forecast (error-

free prediction of rainfall time series). The benchmark results represent the upper limit of the data volume return with respect to which all other estimation methodology should be compared. The benchmark and estimation methodologies are applied to a simulated BC spacecraft pass on Nov. 8, 2022 (starting at 07:59, ending at 16:05 and discretized with a pass of one minute), derived from BC ephemeris data, which is attributed to the corresponding day in 2012 where meteorological measurements are available.

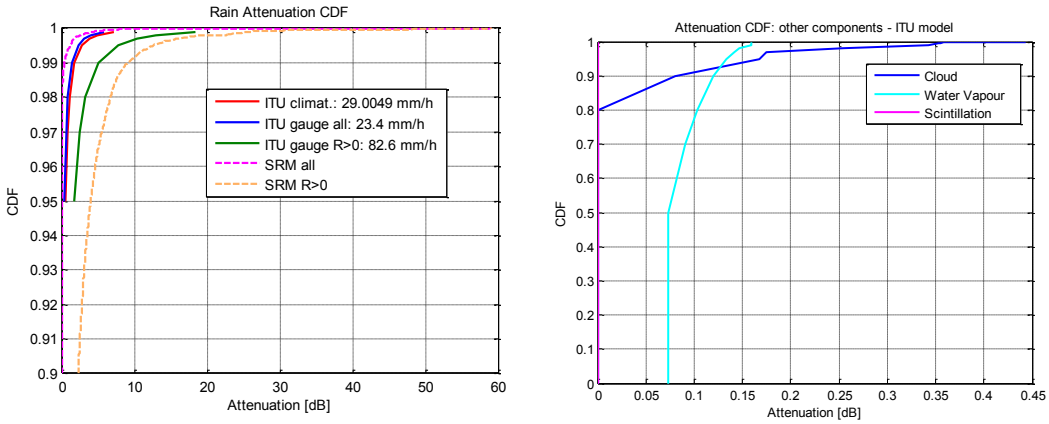

Fig. 3. CDF of yearly attenuation from the probabilistic ITU-R climatological model at Ka band and 90° elevation: total and rain attenuation compared with Cebreros data (left) and other components such as cloud, water vapour and scintillation (right). ITU-R and SRM rain CDFs using Cebreros gauge data (selecting proper R_{001} for ITU, as reported in the legend, and $R \geq 0$ or $R > 0$ for SRM) are also shown in the left panel.

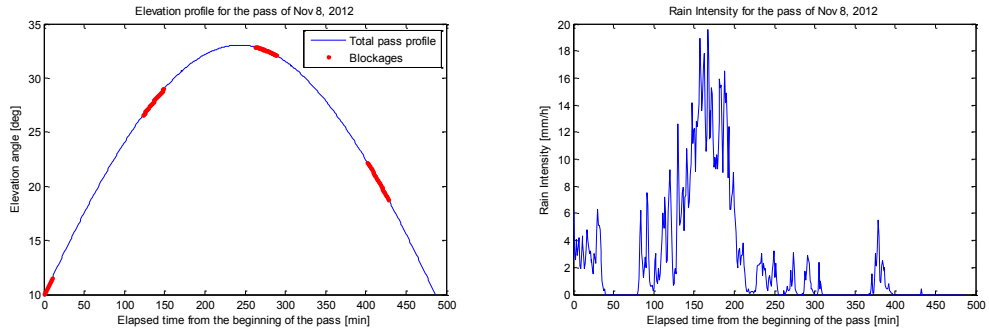

Fig. 4. Time series of elevation angle profile (left panel) and measured rain intensity (right) using Cebreros data of Fig. 1. The BC pass is on Nov. 8, 2022 and is assumed to be arbitrarily valid for Nov. 8, 2012.

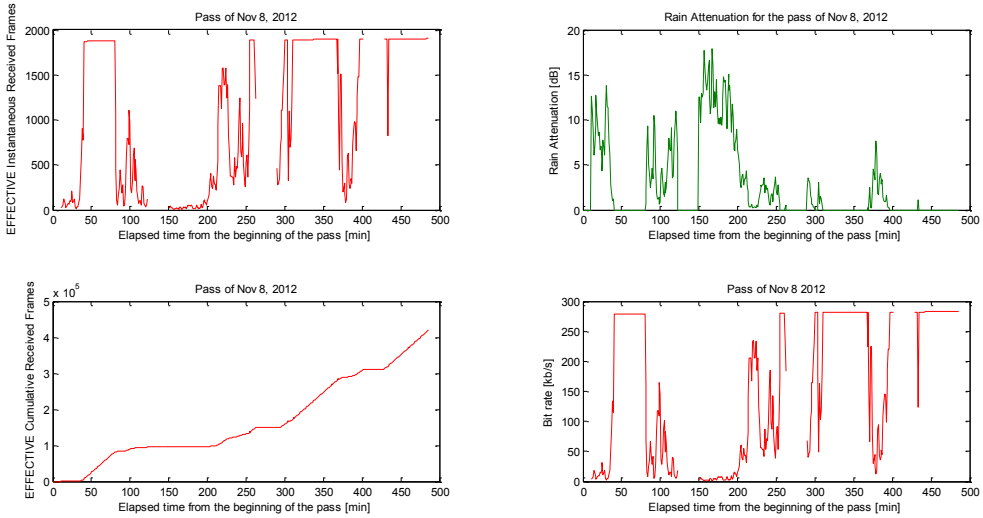

Fig. 5. Time series of effective instantaneous received frames (top left panel), rain attenuation (top right), effective cumulative received frames (bottom left) and optimal bit rate R_b (bottom right) using Cebreros data of Fig. 5 and the benchmark approach with no constraints and a perfect forecast. The BC pass is on Nov. 8, 2022 and is assumed to be arbitrarily valid for Nov. 8, 2012.

The benchmark test-case methodology results are shown in Fig. 5. The elevation temporal profile of about 8 hours is characterized by some expected blockages thus identifying 4 sub-passes. The simplifying assumption is to assume a constant R_b within the whole pass and the minimum elevation equal to 10°. Both the effective instantaneous and cumulated received frames are evaluated by using the near real-time adaptive R_b.

The estimation of the received frames using the conventional and statistical approach is shown in Fig. 6. Note that the transmitting bit rate R_b is constant and, as expected, is equal for both methodologies. However, the expected received frames are different due to the differences in the estimation formulas in (12) versus (16). Table 2 reports the expected number of received frames for all methodologies. Note that the lost frames for the statistical approach is higher than zero due to the statistics of rain path attenuation which is taken into account (see (14) and (15)).

Similarly to Fig. 5, by using the optimal R_b for both conventional and statistical methodologies, it is worth computing the effective number of received and lost frames using the cascade of (1), (5) and (6) using the test case of Fig. 4 and SRM outputs. This result is shown in Fig. 7 where is interesting to observe the behaviour of the received frames are very often zero due to the overestimation of R_b and underestimation the rain path attenuation (which is also elevation dependent) providing an effective ENR below the allowed margin.

The error between the effective (Fig. 7) and expected (Fig. 6) number of received frames is computed in Table 3. In this respect, both approaches underestimate the effective lost frames between 36% and 39% being the conventional approach worse than the statistical approach. As already mentioned, the received frames for both estimation approaches are significantly overestimated due to the assumption of negligible clear-air effects which actually might produce a zenith path attenuation between 0.286 and 0.633 dB [3].

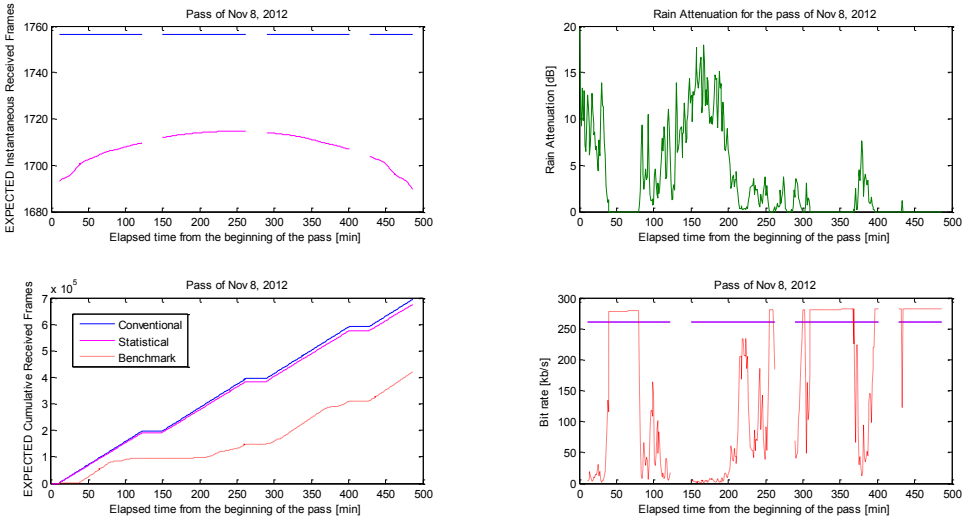

Fig. 6. Same as in Fig. 5, but for ***expected*** frames derived from the conventional and statistical estimation approaches whose bit rate R_b results are coincident in this test. Benchmark results are also shown in the bottom left and right panels.

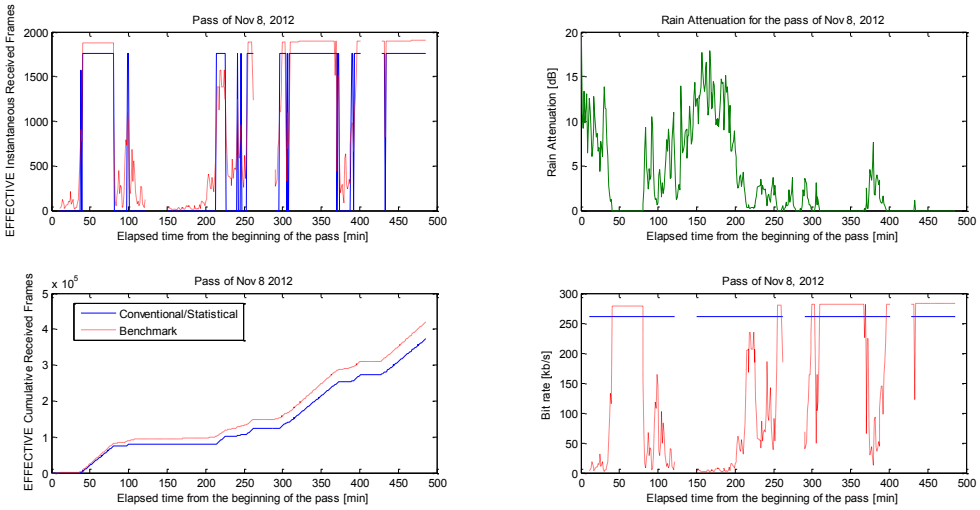

Fig. 7. Same as in Fig. 5, but for ***effective*** frames derived from the constant bit rate R_b estimated from the conventional and statistical estimation approaches (note R_b is the same for both approaches). Benchmark results are also shown.

Table 2. Received frames within the Nov. 8, 2022 pass using different estimation methods.

METHODOLOGY	Elevation θ_m [°]	Bit rate R_b [bps]	Expected F_{RX}	Expected F_{LX}	Expected $F_{LX\%}$ [%]
Conventional	10°	174060	462469	0	0%
Statistical	10°	174060	453850	8619	1.86%
Benchmark	10°	variable	401353	0	0%

Table 3. Comparison of effective and expected received frames using different methods.

METHODOLOGY	Effective F_{RX}	Effective F_{LX}	Effective $F_{LX\%}$	F_{RX} Error	F_{LX} Error	F_{LX} Perc.Error [%]
Conventional	284885	177584	38.4%	177584	-177584	-38.4%
Statistical	284885	177584	38.4%	168965	-168965	-36.54%
Benchmark	401353	0	0%	0	0	0%

VI. CONCLUSIONS

This paper has introduced the concept of the RadioMetOP (RadioMeteorological Operations Planner) technique and described its main modelling components and objectives. Numerical results, in terms of received frame data for constrained and unconstrained system scenarios for 2 estimation methodologies, have been also described together with a discussion about the possible impact of the RadioMetOP method on BepiColombo spacecraft operations. Once established and built the simulation environment, other estimation methodologies (e.g., maximization with sub-pass bit rate variability and parametric minimum elevation angle [5]) can be devised and compared in a homogeneous way, taking the benchmark test case as a reference.

A further step in the optimization of science data return at frequency band higher than X band is to exploit the forecast capability of numerical weather prediction (NWP) models which, coupled with proper radio-propagation microphysical parameterization, can provide the Ka-band average received frames within a deep-space satellite pass (or sub-pass) [10]. The advantage of this approach is to cope with the most probable radio-meteorological situation during the foreseen data transfer instead of relying on a long-term (monthly or yearly) statistics which can strongly penalize the available link margin. On the other hand, as any NWP models, forecast errors should be taken into account especially for what concerns the space-time prediction of atmospheric convective precipitation. Indeed, the accurate forecast of clear weather in a climatologically dry site, like Cebreros, can be even more important for deep-space data volume return optimization.

ACKNOWLEDGEMENTS. This work has been funded by the European Space Agency (ESA) under the contract ESOC-2013 “Study of Ka-band downlink operation concept for BepiColombo based on the use of weather forecasts”.

VII. REFERENCES

[1] E. Matricciani, “An optimum design of deep-space downlinks affected by tropospheric attenuation”, *Int. J. Satell. Commun. Network*, DOI: 10.1002/sat, 2009.

[2] S. Shambayati, “Ka-Band Telemetry Operations Concepts: A Statistical Approach,” Proc. of IEEE, Vol. 95, No. 11, pp 2171-2179, November 2007.

[3] F. Davarian, S. Shambayati, S. Slobin, “Deep space Ka-band Link Management and Mars Reconnaissance Orbiter: Long Term Weather Statistics versus Forecasting,” Proc. of IEEE, Vol. 92, No. 12, pp. 1879-1894, December 2004.

[4] F.S. Marzano, V. Mattioli, C. Capsoni, E. Matricciani, C. Riva, M. Luccini, N. Pierdicca, L. Pulvirenti, M. Montopoli, A. Puiatti, G. Corti, P. Basili, A. Martellucci “Sky-Noise Temperature Modeling and Prediction for Deep Space Applications From X Band to W Band”, Proc. of TTC Conference, Nordwijk (NL), 21-23 Sept. 2010.

[5] M. Montagna, M. Mercolino, M. Arza, M. Lanucara, E. Montagnon, E. Vassallo, M. Media, S. Gmbh, ESA, “Maximisation of data return in Ka-Band for interplanetary missions”, Proc. of TTC Conference, Nordwijk (NL), 21-23 Sept. 2010.

[6] J. Benkhoff, J. Casteren, H. Hayakawa, M. Fujimoto, H. Laakso, M. Novara, P. Ferri, H.R. Middleton, R. Ziethe, “BepiColombo—Comprehensive exploration of Mercury: Mission overview and science goals” , Planetary and Space Science, vol. 58, n. 1-2, p. 2-20, 2010.

[7] G. Brussaard and P.A. Watson, *Atmospheric modelling and millimetre wave propagation*, Chapman & Hall, London (UK), 1995.

[8] F.S. Marzano, “Predicting antenna noise temperature due to rain clouds at microwave and millimeter-wave frequencies,” *IEEE Trans. Antennas and Propagat.*, vol. 55, n. 7, pp. 2022-2031, 2007.

[9] Faccani C., D. Cimini, F.S. Marzano and R. Ferretti, “Three-dimensional variational assimilation of Special Sensor Microwave/Imager data on mesoscale weather prediction model: a case study “, *Q. J. R. Meteorol. Soc*., ISSN: 0035-9009, vol. 133, pp. 1295-1307, 2007.

[10] International Telecommunication Union – Radiopropagation (ITU-R), “Propagation data and prediction methods required for the design of Earth-space telecommunication systems”, ITU-R. REC. P. 618-10.